Effects of wheelset flexibility on the simulation of vehicle-track interaction at crossings

Shen, C; Wei, Z; Burgelman, NDM; Dollevoet, RPBJ; Li, Z

DOI
10.1201/b21185-165

Publication date
2016

Document Version
Accepted author manuscript

Published in
Proceedings of the 24th international symposium on dynamics of vehicles on roads and tracks, IAVSD 2015

Effects of wheelset flexibility on the simulation of vehicle-track interaction at crossings

C. Shen, Z. Wei, N. Burgelman, R. Dollevoet and Z. Li
Section of Railway Engineering, Faculty of Civil Engineering and Geosciences, Delft University of Technology, Delft, The Netherlands

ABSTRACT: Though numerical models based on multi-body dynamics (MBD) are often used to simulate the vehicle-track interaction at crossing impact, their relative capabilities and accuracy were not discussed. This paper aims to investigate the influence of wheelset flexibility on the result of crossing impact simulation in the frequency range 0~500Hz. Two models are used: a MBD model with rigid wheelset and a reference finite element model that could fully account for the structural flexibility. Results of the two models as well as in-situ measurement show three characteristic frequencies of the vehicle-track interaction system induced by crossing impact. Based on the characteristic frequencies, the MBD model is tuned to resemble the reference FE model in terms of track and contact representation through a parametric analysis so that the influence of these differences can be isolated. It is found that the major influence of the wheelset flexibility is on the second characteristic frequency of the system, reflecting the second order bending of the wheelset.

1 INTRODUCTION

The degradation and damage of switches and crossings (S&C, turnouts) are crucial problems in railway systems as they could result in high maintenance cost. This high cost is mainly attributed to the high vehicle-track interaction force at S&C, which is much more severe than that at tangent tracks, especially in the case that the wheel impacts on the crossing nose. Therefore, it is of great importance to accurately model the vehicle-track interaction at S&C, both in the nominal and the degraded state. Such a model could be utilized to quantify the relationships between the dynamic responses and the actual state of the S&C. The understanding of these relationships could facilitate early detection of S&C degradation, which allows for preventive maintenance and thus reduces the maintenance cost.

This paper focuses on low to medium frequency, i.e. up to 500Hz. Such vibrations are most likely related to the nominal S&C geometry and structural stiffness/inertia or if the nominal state is disturbed, the degradation of S&C components, such as loose bolts, breakage in fastening systems, hanging sleepers, settlement in the ballast or the subgrade etc. For this purpose, a multi-body dynamic (MBD) method is most appropriate especially when the vehicle dynamic response (e.g. axle box acceleration, ABA) is desired as the output.

Effective modelling of three parts: track, vehicle and wheel/rail contact, is required both in terms of accuracy and computational effort for MBD method. Though different MBD models in terms of the abovementioned three aspects have been developed to investigate the vehicle turnout interaction (e.g. flexible track model with rail modal shapes(Kassa and Nielsen, 2009), flexible wheelset model(Bruni et al., 2009), flexible track model with rail beams(Markine et al., 2011), contact model WEAR(Burgelman et al., 2014), moving track model(Pålsson and Nielsen, 2015), etc.), the influence of the different modelling methods on their relative capabilities and accuracy is not discussed.

The influence of different vehicle models, in particular the modelling of wheelset flexibility, is of special interest for the current paper. With a flexible representation, the wheelset resonances at certain frequencies can be considered and they will lead to deviations in simulation results. For tangent tracks, the effects of using flexible wheelset models on the simulation of vehicle-track interaction have been studied intensively under different loading conditions (Chaar and Berg, 2006, Torstensson et al., 2011, Casanueva et al., 2012). The general conclusion is that the necessity and complexity of the flexible wheelset model depend on the type of excitation to which it is subjected. Under certain excitations, for example a wheelflat impact , including more flexible modes will not necessarily lead to noticeable improvement in accuracy, whereas it will inevitably add to the computational effort. For the crossing impact, however, the effects of wheelset flexibility have not yet been investigated. On one hand, the excitation characteristics of the impact in terms of major frequency contents are not reported in the literature so far. On the other hand, the abovementioned flexible wheelset models are all based on modal superposition of which the accuracy largely depends on the number of mode shapes that are included in the model. Such simplification might jeopardize its reliability when serving as a reference model.

Furthermore, the effects of wheelset flexibility are generally evaluated by contact forces (Chaar and Berg, 2006), track dynamics (Bruni et al., 2009) and vehicle stability (Casanueva et al., 2012). Its effects on ABA have not been investigated. Predicted ABA will serve as the indicator to evaluate the effects of wheelset flexibility so that in future studies the ABA characteristics obtained from real-life measurements and predicted by the model can be correlated for validation of the model and subsequently help better understand train-S&C interaction and the resulting S&C degradation.

This paper presents a comparison between an MBD model with rigid wheelset and a reference FE model with flexible wheelset regarding the simulation results of the vehicle-track interaction during crossing transition. The characteristic frequencies of ABA and excited track modes are first identified. Accordingly, the MBD model is calibrated with the FE model to yield the similar track and contact representation through a parametric analysis. Finally, the effects of wheelset flexibility are presented using the calibrated MBD model.

2 MODELLING AND MEASUREMENT METHODS

Two models are employed in this paper. The first is an FE model with detailed modelling of the wheelset flexibility and the wheel-rail contact. By validating the FE model with measurement, it serves as a reference. The other model is based on MBD without accounting for wheelset flexibility, but including detailed modelling of the vehicle. It is expected that by comparing the results of the two models the effects of wheelset flexibility can be clarified.

In the FE model, a right-hand turnout of the 54E1-195-1:9 type with a nominal rail profile UIC54 is presented with the rails and sleepers modelled with solid elements, the railpads and ballast modelled with spring/damper elements, as shown in Figure 1. The vehicle model is simplified: only one wheelset is included, modelled with solid elements; the car body and bogie are represented by a single lumped mass, connected to the wheelset with springs and dampers representing the primary suspension. To account for the plastic deformation of the wheelset and the rail, a bilinear kinematic strain hardening elasto-plastic material model is employed. One of the major advantages of this model is that the flexibility of the wheelset, as well as the track, can be fully considered as they are modelled with solid elements instead of beams or mode shapes. Additionally, the lateral and yaw motion of the wheelset can be prescribed as is obtained from in-situ measurement or from vehicle dynamics simulation so that the movement can also be modelled more realistically. The detailed description and capability of the model can be found in a separate paper (Wei et al., in prep.).

The second model, using the MBD method, considers the wheelsets as rigid bodies. A conventional moving-track model is used, where the rails and sleepers are represented by individual masses and connected by linear spring dampers and move with the wheels, as shown in Figure 2(a). A three-dimensional Cartesian coordinate is adopted in this study, of which the axes x, y, and z is oriented in the longitudinal, lateral and vertical directions, respectively. Only vertical and roll motions about the x axis are allowed for the masses representing rails and sleepers. This kind of model is widely used in the modelling of vehicle turnout interaction, especially in opti-

mization or parametric studies (Pålsson, 2013, Wan et al., 2014); the main advantage is the computation time which is much shorter compared to other methods. The rail profile change along the longitudinal direction is considered by sampling the lateral cross section of the FE model at every 14mm intervals, see Figure 2(b). The track model only considers the through route of the turnouts, which means the sleepers are half in length compared to those in the FE model. The vehicle is modelled as simple as possible to resemble the vehicle model in the FE model. Only one car body and two wheelsets are included as rigid bodies, connected by spring/damper representing the vertical primary suspension. As for the contact model, a multi-Hertzian/Fastsim approach is adopted.

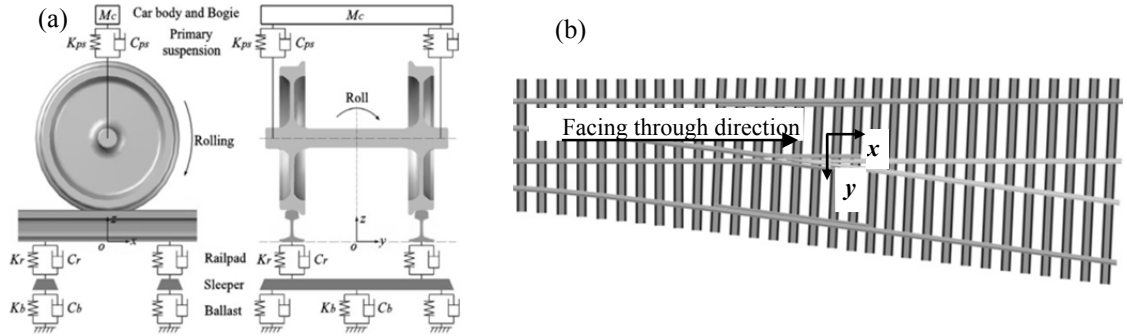

Figure1. FE model. (a) Vehicle-track interaction system; (b) Track model(top view).

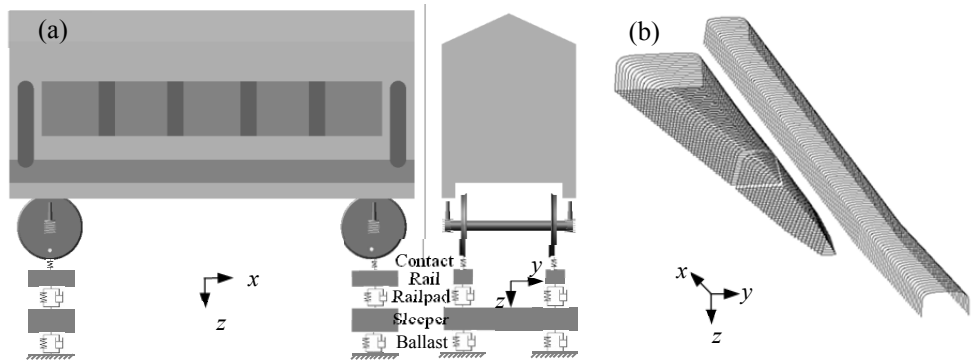

Figure 2. MBD model. (a) Vehicle-track interaction system; (b) Crossing nose geometry.

The major input parameters for the MBD are listed in Table 1. The mass and inertia properties are calculated from the FE model. The stiffness and damping parameters of the railpad and ballast are also the same as in the FE model which are derived from hammer tests at several locations of Dutch railway network (Oregui et al., 2015).

For comparison, in-situ measurement of the ABA signals of a vehicle passing the crossing panel along the through-route and facing move direction were acquired with accelerometers mounted on vehicle axle boxes. The vehicle speed was 21m/s and the sampling frequency was 25600Hz. The measurements were made twice to ensure repeatability. The same scenario is simulated with both models at a sampling frequency of 10000Hz for the computed ABA.

Table 1. Parameters for MBD model.

Track		
Rail	Mass (kg)	54
	Moment of inertia I_{xx} (kg m^2)	0.22307345
Railpad	Vertical stiffness(MN/m)	1560
	Damping(kNs/m)	67.5
Sleeper	Mass (kg)	244
	Moment of inertia I_{xx} (kg m^2)	137
Ballast	Vertical stiffness(MN/m)	90
	Damping(kNs/m)	64

Vehicle		
Wheelset	Mass (kg)	1120
	Moment of inertia I_{xx} (kg m^2)	640
Primary suspension	Stiffness (MN/m)	1.15
	Damping (Ns/m)	2500

3 RESULT

3.1 *Characteristic frequencies*

Time history of ABA from the measurements and the simulations with a low pass filter of 1000Hz are shown in Figure 3(a)~(d). The signals are truncated to 0.07 seconds long and the impact occurs at the first peak of the signal. Wavelet transform is applied to the each of the time domain signals and the plots of wavelet power spectrum (WPS)(Molodova et al., 2013), i.e. scalograms, are shown in Figure 3(e) ~(h). The WPS is evaluated as $|W^2(s,\tau)|$, where W(s,τ) represents the wavelet coefficient. The global wavelet spectrum (GWS), defined as the wavelet power averaged over the time at different frequencies, is also calculated, see Figure 4.

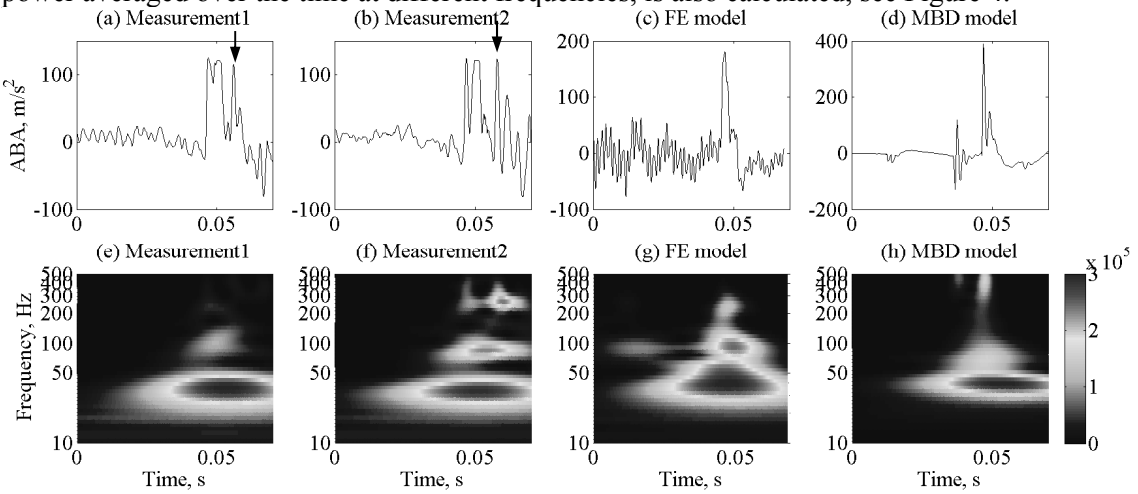

Figure 3. Time domain signals and scalograms of ABA

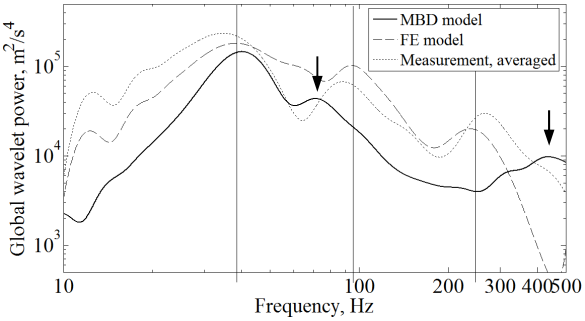

Figure 4. Global wavelet spectrum of ABA signals

Several observations can be made:

The result of FE model yield better match with the measurement both in terms of frequency content and magnitude than the MBD model. This indicates the reliability of the FE model as a reference model.

Comparing the FE result with the measurement, three major characteristic frequencies can be identified at around 40Hz, 100Hz and 250Hz. With the vehicle speed of 21m/s, the corresponding wavelengths are approximately 0.52m, 0.21m and 0.08m, respectively, as shown in Figure 4 with the three vertical bars.

The MBD model well reproduces the first characteristic frequency at 40 Hz compared to the measurement and the FE model. However, the second characteristic frequency is lower at around 70 Hz and the third is higher at 450 Hz, as indicated by the arrows in Figure 4. As the MBD model employs the same input parameters as the FE model, the output differences should result from the modelling differences in track representation, contact method or vehicle model. This will be discussed in detail later in this paper.

Both models are not able to reproduce the peaks after the impact, as indicated by the arrows in Figure 3 (a)(b). These peaks feature the frequencies from 250 Hz to 300Hz (wavelength 70~80mm), which could be the result of crossing surface geometry irregularities that are not included in both models.

3.2 *Exited track modes*

A linear modal analysis is performed on the FE model to identify the exited track modes during the crossing transition. Track modes corresponding to the characteristic frequencies are shown in Figure 5. Note that the deviation of the first full track mode at 70 Hz from the first characteristic frequency at 40 Hz might be due to the different loading conditions. The frequency of the first full track mode is lower at loaded condition(Molodova, 2013). The first two resonances are full track vibrations while the third one involves bending of the sleepers. These identified track modes can be used to further calibrate the track model in the MBD method.

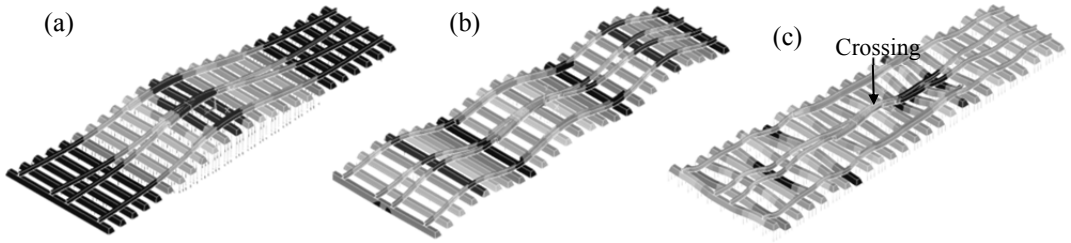

Figure 5. Exited track modes in the FE model. (a)70Hz; (b)100Hz; (c)250Hz

For the MBD model, the vertical vibration modes of the track can be identified by comparing the vertical movement of the axle box with the vertical movement of the sleeper, as shown in Figure 6(a). The impact occurs at 3.1s. Immediately after the impact, the axle box and the sleeper moves in the opposite direction. After about 0.01 seconds, the two parts start to vibrate in phase, of which the frequency is around 40 Hz. This represents the full track modes of the MBD model and it is the same as the FE model. Figure 6(b) presents the vertical acceleration of the axle box and the sleeper bandpass filtered by 200Hz~1000Hz. The two parts vibrate anti-phase at the third resonance frequency, i.e. 450Hz, corresponding to the anti-sleeper resonance of the track. Normalized GWS of the vertical acceleration of the sleeper is calculated by dividing the global wavelet power at each frequency by the maximum wavelet power, as shown in Figure 6(c). Two distinct peaks are observed at around 40Hz and 450Hz, corresponding to the full track and anti-sleeper modes described above.

The second resonance observed in the MBD model at around 70Hz does not reflect any vertical track modes. It originates from the rotation of the sleeper about the x axis. The normalized rotational acceleration of the sleeper and the vertical ABA bandpass filtered by 50Hz~90Hz are presented in Figure 7(a). It can be seen that the sleeper rotates with the vertical movement of the axle box at the same frequency with a phase shift. Figure 7(b) shows the normalized GWS of the rotational acceleration of the sleeper. The peak at around 70Hz represents the vibration shown in Figure 7(a). Another two peaks that are related to the sleeper rotation are observed at 220Hz and 310Hz, which cannot be found in the ABA response (see Figure 4). However, it will be shown in Section 4 by tuning the parameters of the system that, these two frequencies can also be excited in the ABA signal.

The three track modes excited in the MBD model are full track mode, sleeper rotational mode and anti-sleeper mode, as shown in Figure 8, corresponding to the frequencies of 40Hz, 70Hz and 420Hz, respectively. Besides, another two modes related to the sleeper rotation are not reflected in the ABA signal with the current model parameters.

Compared to the track modes shown in Figure 5, only the first full track mode of Figure 5(a) is reproduced. As the MBD method uses co-following individual masses instead of continuous solid/beam elements to represent rails, it is not possible to simultaneously reproduce the second full track mode indicated in Figure 5(b). The bending of the sleeper at the crossing nose shown in Figure 5(c) can be resembled by the rigid rotation of the whole sleeper about the *x* axis in the MBD model shown in Figure 8(b), as the sleeper in the MBD model is half in length compared to that in the FE model. This can be achieved, as will be shown later in Section 4, by tuning the pertinent track parameters to shift the sleeper rotation frequency from 70Hz to 220Hz. Besides, the anti-sleeper resonance in Figure 8(c) should be eliminated as it is neither excited in the FE model nor observed in the measurement.

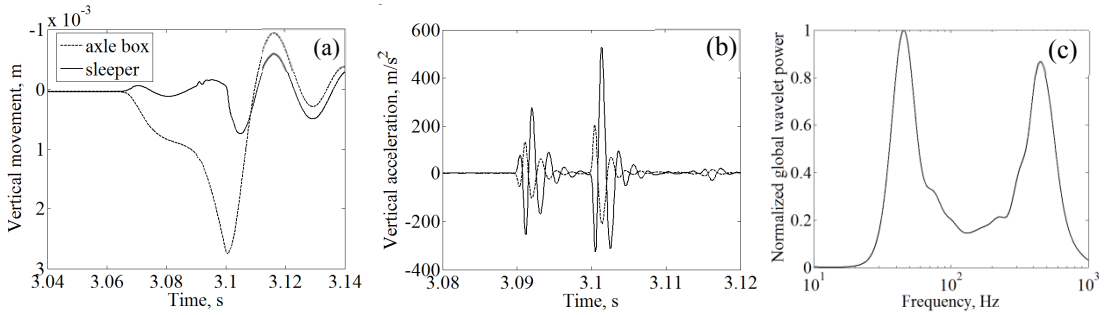

Figure 6. Vertical track vibration in the MBD model.(a) 40 Hz; (b)450 Hz; (c) Normalized GWS.

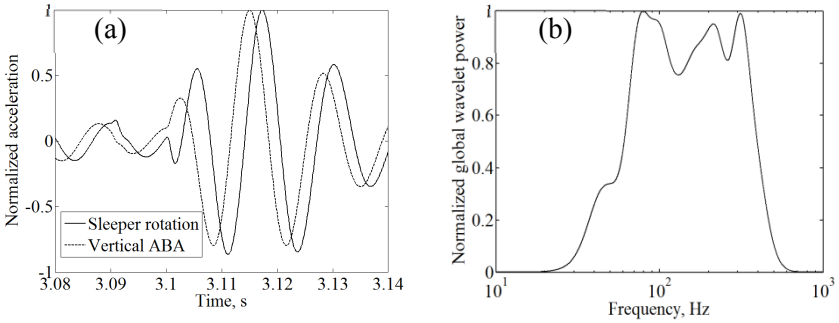

Figure 7. Rotational track vibration in the MBD model.(a) 70Hz; (b) Normalized GWS.

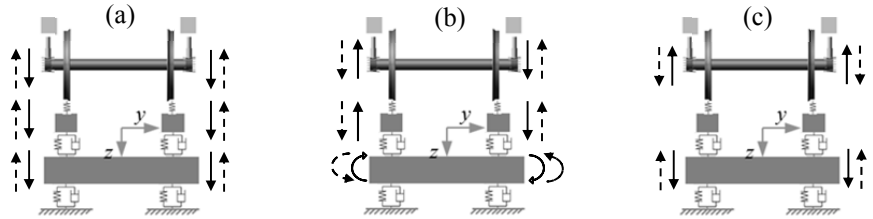

Figure 8. Exited track modes in the MBD model.(a) Full track: 40Hz;(b) Sleeper rotation: 70Hz; (c) Anti-sleeper: 450Hz.

4 PARAMETRIC ANALYSIS

Ideally, to serve the purpose of this research, the two models should be exactly the same except for wheelset flexibility. However, this is not possible owing to the respective capability of the models.. Besides the wheelset flexibility, several other differences exist, such as the contact solution and the track model which are both modeled simpler in the MBD model than in the FE model.

Nevertheless, each of the differences corresponds to different component in the vehicle-track interaction system, while each of the components plays a unique role in the system and hence corresponds to unique characteristics in the dynamic responses. Therefore, by varying the parameters of the system, the influences of the differences in the models can be isolated.

4.1 *Track model*

In this section, track parameters that correspond to different characteristic frequencies are classified. Based on that the MBD model is tuned to yield the same track representation in terms of the major frequency characteristics as the FE model so that the differences in track models can be either ruled out or clarified.

Figure 9 shows the track parameters that influence the first characteristic frequency. With lower ballast stiffness or heavier sleeper, the magnitude at the first characteristic frequency reduces and the peak shifts to lower frequencies. This can be explained by simplifying the track system to a single degree of freedom system as this characteristic frequency corresponds to the first full track modes, in which sleeper and rail moves in phase in the vertical direction. Decreasing the stiffness or increasing the mass of the system will result in lower natural frequency as well as lower dynamic stiffness. The results confirm the argument that frequency at 40Hz reflects the full track vibration.

Figure 10 shows the track parameters that influence the second and the third characteristic frequencies. Rail mass only influences the GWS magnitude at 450Hz whereas tuning railpad stiffness and sleeper mass can also lead to the shift of this frequency, see Figure 10(a)~(c). The new resonance frequencies in Figure 10(a) and (c) are either 220Hz or 310Hz, which agree with the two rotation resonances of the sleeper shown in Figure 7. This indicates that by changing the railpad stiffness or sleeper mass the anti-sleeper vibration is depressed while the rotational vibration of the sleeper is excited.

Increasing the sleeper moment of inertia about the x axis manifests a decrease of GWS at 70Hz as well as an increase of GWS at 220Hz while the GWS magnitude at the anti-sleeper resonance frequency remains almost the same, as shown in Figure 10(d). Therefore, varying the sleeper moment of inertia has little influence on the anti-sleeper vibration whereas shifts the rotational vibration of sleeper from 70Hz to 220Hz.

4.2 *Contact model*

Plastic deformation at crossing impact can be considered in the FE model while the MBD model adopts Hertzian contact based on elastic body assumption. Figure 11(a) shows a comparison between the results of two FE models with either plastic or elastic material. Higher power is predicted by the elastic FE model in the high frequency range (above 400Hz) as the energy can be dissipated through plastic deformation at contact in the plastic FE model.

Such energy dissipation cannot be properly modelled in the MBD model. An alternative way is to decrease the total input energy by changing the Hertzian contact stiffness. The Hertzian contact stiffness is altered by changing the Young's modulus of the rail. It can be seen from Figure 11(b) that the original anti-sleeper resonance is significantly reduced when using lower Hertzian contact stiffness. This is because with lower contact stiffness the high frequency components of the contact force are less and hence the energy input through the contact to the track system is concentrated below the anti-sleeper frequency (450Hz in this case).

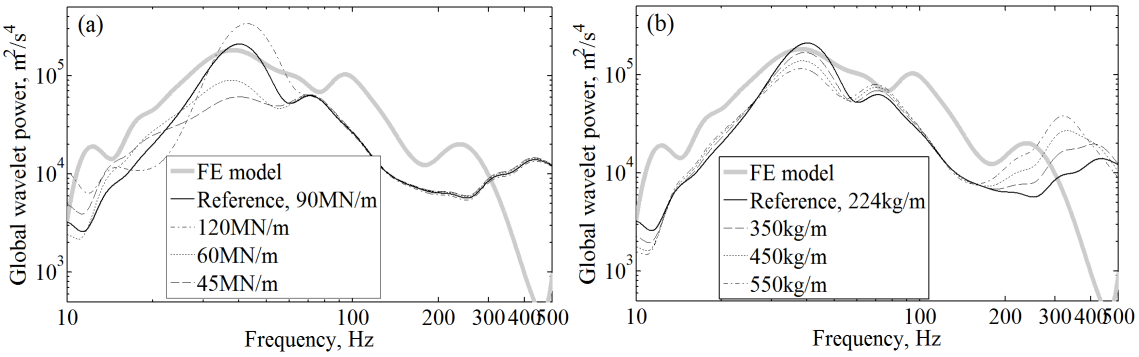

Figure 9. Parameters corresponding to the first characteristic frequency(a)Ballast stiffness;(b) Sleeper mass.

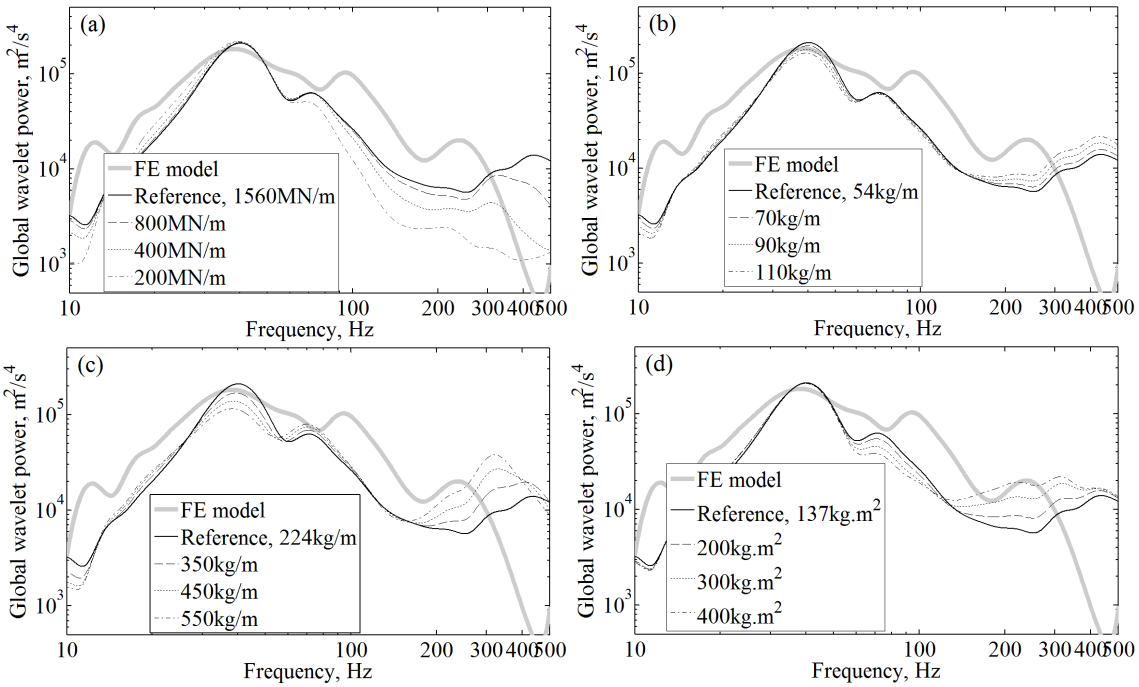

Figure 10. Parameters corresponding to the second and third characteristic frequencies. (a)Rail pad stiffness;(b)Rail mass;(c)Sleeper mass;(d)Sleeper moment of inertia.

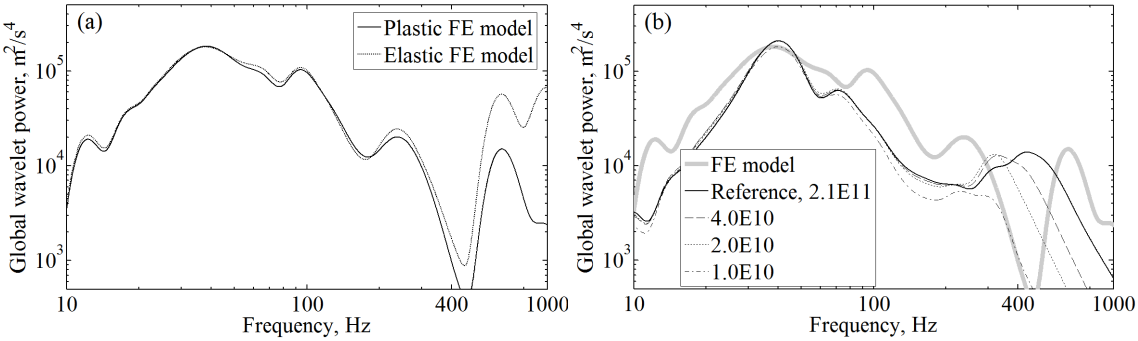

Figure 11. Influence of contact model (a) Plastic and elastic material models;(b) Hertzian contact stiffness

5 EFFECTS OF WHEELSET FLEXIBILITY

5.1 *Mode shapes of wheelset*

Modal analysis is also performed to identify the mode shapes and corresponding frequencies of the wheelset in the FE model. As only the vertical ABA below 500Hz is of interest in this paper, the first three bending modes of the wheelset are shown, see Figure 12.

(a) 71.3Hz (b)115.7Hz (c) 256.2Hz

Figure 12. First three bending modes of the wheelset in the FE model.

5.2 *Excitation simulation*

With the calibrated MBD model, time history of the vertical wheel-rail interaction forces on both wheels during crossing transition can be obtained. They are then applied to the flexible FE wheelset model as excitations, see Figure 13. Characteristic frequencies corresponding to the track and contact in the calibrated MBD model are reflected in the contact forces and hence in

the excitations to the flexible wheelset model. By comparing the ABA of the two models, the effects of the wheelset flexibility can be clarified.

The results are shown in Figure 14. Time history of the vertical ABA of both models shows good agreement, see Figure14(a), except for the fact that more high frequency oscillations are observed in the FE result. In the frequency domain, the first and the third characteristic frequencies at 40Hz and 230Hz in the calibrated MBD model are also pinpointed in the flexible wheelset model. The second characteristic frequency at 70Hz in the calibrated MBD model shifts to 115Hz in the flexible wheelset model, which is close to the second resonance frequency (100Hz) in the FE model. Therefore, it is possible that the second characteristic frequency observed in the FE model and measurement is also related to the flexible wheelset. It is also observed that the introduction of wheelset flexibility reduces the global wavelet power in the frequency range 50~90Hz. The reason for the reduction needs further investigation in future studies.

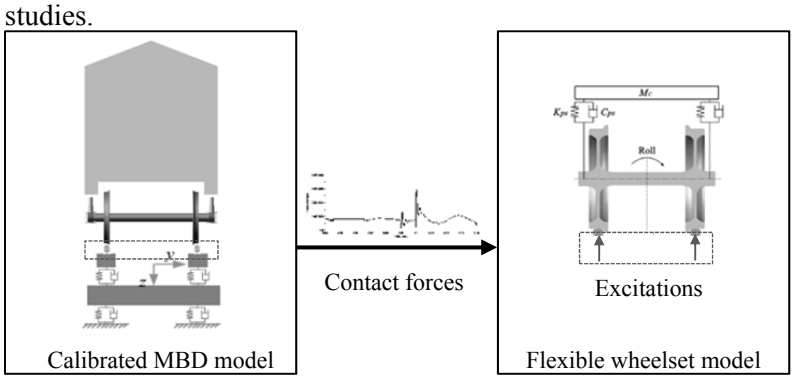

Figure 13. Methodology for excitation simulation.

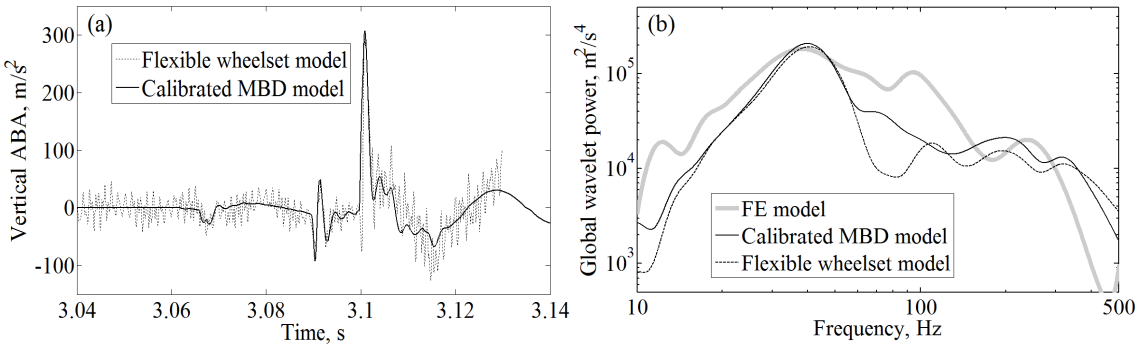

Figure 14. Results of excitation simulation.(a) Time domain; (b)Frequency domain.

Figure 15 shows the response of the flexible wheelset under different excitations. The excitations derived from the original MBD model and the calibrated MBD model are used. Results show the second characteristic frequency remains the same at 115 Hz regardless of the different excitations. This is because this frequency is induced by the flexible bending modes of the wheelset. As the impact loads on the two wheels are asymmetric, only the asymmetric wheelset bending mode is excited. Besides, the third frequency changes according to the excitation, which indicates it is generated by the excited track modes.

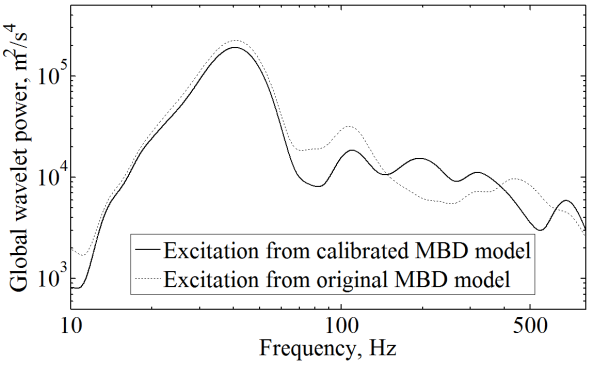

Figure 15 Flexible wheelset responses subjected to different excitations

6 SUMMARY AND FUTURE WORK

This paper compares an MBD model with rigid wheelset and moving track representations with an FE model that can fully account for the structural flexibility. The FE model is verified through in-situ ABA measurement so that it is taken as the reference. By calibrating the MBD model to yield similar track and contact representations as the FE model, the influence of the wheelset flexibility is identified. Major conclusions are:

(1) One of the limitations of the moving track model is that its use of co-following individual masses instead of continuous solid/beam elements to represent rails cannot reproduce the second full track mode identified in both the measurement and FE model. Besides, rigid and half-length sleeper model will induce variations in track modes relating to bending and rotation of the sleeper. As to Hertzian contact model, it predicts higher energy in high frequency contents as the energy cannot dissipate through plastic deformation.

(2) Calibration is needed because the abovementioned assumptions in the MBD model. However, it is only valid in the situation investigated in this paper, i.e. wheel-crossing impact. In this regard, the FE model is more reliable as its assumptions are much fewer.

(3) The introduction of wheelset flexibility in the current MBD model leads to a new resonance at 115Hz which is caused by the asymmetric second bending mode of the wheelset.

The limitations of the current MBD model can be improved by using a flexible track model in future studies. A comparison between different track models to investigate their capabilities and accuracy is also necessary. Besides, appropriate and efficient contact and flexible wheelset representations are needed for the MBD method to accurately describe the dynamic behavior of crossing impact. Considering FE method alone is too time-consuming, coupling of FE with MBD method seems to be a promising way.

REFERENCES

BRUNI, S., ANASTASOPOULOS, I., ALFI, S., VAN LEUVEN, A. & GAZETAS, G. 2009. Effects of train impacts on urban turnouts: Modelling and validation through measurements. *Journal of Sound and Vibration,* 324**,** 666-689.

BURGELMAN, N., LI, Z. & DOLLEVOET, R. 2014. A new rolling contact method applied to conformal contact and the train-turnout interaction. *Wear,* 321**,** 94-105.

CASANUEVA, C., ALONSO, A., EZIOLAZA, I. & GIMENEZ, J. G. 2012. Simple flexible wheelset model for low-frequency instability simulations. *Proceedings of the Institution of Mechanical Engineers, Part F: Journal of Rail and Rapid Transit,* 228**,** 169-181.

CHAAR, N. & BERG, M. 2006. Simulation of vehicle–track interaction with flexible wheelsets, moving track models and field tests. *Vehicle System Dynamics,* 44**,** 921-931.

KASSA, E. & NIELSEN, J. C. O. 2009. Dynamic train–turnout interaction in an extended frequency range using a detailed model of track dynamics. *Journal of Sound and Vibration,* 320**,** 893-914.

MARKINE, V. L., STEENBERGEN, M. J. M. M. & SHEVTSOV, I. Y. 2011. Combatting RCF on switch points by tuning elastic track properties. *Wear,* 271**,** 158-167.

MOLODOVA, M. 2013. *Detection of early squats by axle box acceleration*, TU Delft, Delft University of Technology.

OREGUI, M., LI, Z. & DOLLEVOET, R. 2015. An investigation into the modeling of railway fastening. *International Journal of Mechanical Sciences,* 92**,** 1-11.

PÅLSSON, B. A. 2013. Design optimisation of switch rails in railway turnouts. *Vehicle System Dynamics,* 51**,** 1619-1639.

PÅLSSON, B. A. & NIELSEN, J. C. O. 2015. Dynamic vehicle–track interaction in switches and crossings and the influence of rail pad stiffness – field measurements and validation of a simulation model. *Vehicle System Dynamics,* 53**,** 734-755.

TORSTENSSON, P. T., NIELSEN, J. C. O. & BAEZA, L. 2011. Dynamic train–track interaction at high vehicle speeds—Modelling of wheelset dynamics and wheel rotation. *Journal of Sound and Vibration,* 330**,** 5309-5321.

WAN, C., MARKINE, V. L. & SHEVTSOV, I. Y. 2014. Improvement of vehicle–turnout interaction by optimising the shape of crossing nose. *Vehicle System Dynamics,* 52**,** 1517-1540.

WEI, Z., SHEN, C., LI, Z. & DOLLEVOET, R. 2015. Modelling wheel-rail impact-like interaction at crossing panel. In preperation.